Accepted Manuscript

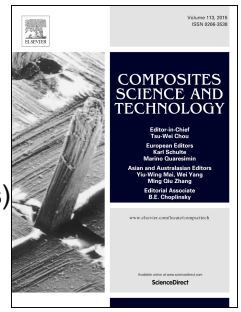

Nanocomposites based on poly(L-lactide)/poly(ε-caprolactone) blends with triple-shape memory behavior: Effect of the incorporation of graphene nanoplatelets (GNps)

Fatemeh KhMolavi, Ismaeil Ghasemi, Massimo Messori, Masoud Esfandeh

PII: S0266-3538(17)31411-2

DOI: 10.1016/j.compscitech.2017.08.021

Reference: CSTE 6876

To appear in: *Composites Science and Technology*

Received Date: 12 June 2017

Revised Date: 3 August 2017

Accepted Date: 18 August 2017

Please cite this article as: KhMolavi F, Ghasemi I, Messori M, Esfandeh M, Nanocomposites based on poly(L-lactide)/poly(ε-caprolactone) blends with triple-shape memory behavior: Effect of the incorporation of graphene nanoplatelets (GNps), *Composites Science and Technology* (2017), doi: 10.1016/j.compscitech.2017.08.021.

Nanocomposites based on Poly(L-lactide)/Poly(ε-caprolactone) Blends with Triple-Shape Memory Behavior: Effect of the Incorporation of Graphene Nanoplatelets (GNps)

Fatemeh Kh.Molavi[1, 2], Ismaeil Ghasemi[1*], Massimo Messori[2], Masoud Esfandeh[1]

1. Department of Polymer Processing, Iran Polymer and Petrochemical Institute, P.O.Box:14965/115, Tehran, Iran

2. Department of Engineering "Enzo Ferrari", University of Modena and Reggio Emilia, Via P. Vivarelli 10/1, 41125 Modena, Italy

Corresponding Author: I.ghasemi@ippi.ac.ir

Abstract

In this study, a novel thermally actuated triple-shape memory polymer (triple-SMP) based on poly(L-lactide) (PLA)/poly(ε-caprolactone) (PCL)/graphene nanoplatelets (GNps) nanocomposite was prepared by facile solution mixing method and the design of which was based on two well-separated melting temperatures. In order to improve the dispersion of GNps in the matrix, functionalization reactions were carried out on the GNPs surface. Functionalization was confirmed by various techniques including FTIR, Raman and TGA analysis. TEM micrographs revealed an exfoliated morphology for the functionalized GNps (FGNps) and a homogenous dispersion in the matrix. The crystallinity behaviour of nanocomposites was investigated by DSC and variable temperature XRD (VT-XRD) analysis and an increase in crystallinity was observed. Dynamic mechanical analysis (DMA) showed that the presence of FGNps improves the fixity and recovery ratios because of increase in crystallinity and thermal conductivity. The best shape memory behavior was obtained for PLA50/PCL50/FGNp 1.5 nanocomposite.

Keywords: Nano composites; Polymer-matrix composites (PMCs); Smart materials; Thermomechanical properties.

1. Introduction

Shape memory polymers (SMPs) are smart materials which able to recover to the original (permanent) shape from temporary shapes upon exposure to an external stimulus [1-3]. Typically, SMPs are composed of two different structures: one is fixed domain that is considered as hard segment, the other is reversible domain that is termed as soft segment [4].

SMPs, based on number of temporary shapes, are divided into dual and multiple-SMPs. The multiple-SMPs with two temporary shapes are known as triple-SMPs [5, 6]. There are two strategies for developing the multiple-SMPs materials: the first is to utilize polymers with a broad thermal transition temperature. In this system, glass or melting temperatures can be selected as thermal transition [7-9]. Nochel et al. [10] prepared the covalently cross-linked poly(ethylene-co-vinyl acetate) and the result revealed the existence of the triple shape memory effect due to broad melting transition temperatures. The other kind of strategy is based on immiscible blend including the several domains with well separated thermal transition temperatures [11, 12]. Zhao et al. [11] reported that chemically cross-linked polyethylene (PE)/polypropylene (PP) blends demonstrated triple-SMP. In this system, two crystallization/melting transitions of PE and PP are well separated. The other blend systems including two glass transitions or one crystallization/melting transition and one glass transition are also developed to acquire the triple-SMP [13, 14]. The second strategy for achieving the multi-SMP is more interesting, because in this system by controlling the microstructure, most polymer blends with well separated thermal transitions can show multiple-SMP.

Although SMPs show the ability to change their shape, they also have some disadvantages such as low elastic modulus, strength and strain [15]. To overcome this inherent deficiency, introducing nano fillers such as clay montmorillonite, carbon nanotubes, and so on into polymer matrix to reach SMP nanocomposites is a new strategy [16, 17]. Recently graphene nanoplatelets

(GNps) are used in polymer nanocomposites due to its excellent mechanical, thermal and electrical properties and also because of its low density and high surface area [18-22]. However, according to tendency of GNps to agglomeration and weak interaction with polymeric matrix, several methods have been developed to obtain the efficient dispersion of GNps in matrix, which including surface modification and covalent functionalization [23, 24].

To the best of our knowledge, there is no report about chemically cross-linked triple-SMPs reinforced by GNps. So, here, we reported the preparation, thermo-mechanical properties and triple-shape memory effect of nanocomposite samples based on PLA/PCL. In addition, attempts were made to study the functionalized GNps (FGNps) on the triple-SMPs performance. Regarding to the well-separated melting transition temperatures of phases ($T_{m,\,PLA}$ and $T_{m,\,PCL}$), a new triple-SMP was induced by thermal programming using dynamic mechanical analyzer.

2. Experimental section

2.1. Materials

Poly(L-lactide) (grade 3251D, average molecular weight of 90~120kgmol^{-1}) was supplied by NatureWorks. LLC, USA. Poly(ε-caprolactone) was obtained by Sigma-Aldrich (grade 200, M_n= 80000gmol^{-1}). Graphene nanoplatelets (GNps) were purchased from XG Science, Inc. (Lansing MI, USA) with trade name XGNp-C750 (the average thickness of 1-5nm, length of less than 2µm and surface area 750m^{2}g^{-1}). Nitric acid (68%), sulfuric acid (98%), thionyl chloride ($SOCl_2$), tetrahydrofuran (THF), and N, N-dimethylformamide (DMF) were obtained from Sigma-Aldrich and used for modification of GNps. Dicumyl peroxide (DCP) was supplied by Hercules Korea Chemicals Co., Ltd. and triallyl isocyanaurate (TAIC) was purchased from GO YEN chemical industrial Co., Ltd., Taiwan.

2.2. Graphene nanoplatelets functionalization

To provide oxidized GNp (OGNp), the GNp was added into a 20ml flask containing sulfuric acid (6ml) and nitric acid (2ml) (H_2SO_4/ HNO_3; v:v= 1:3) by method as described in our previous work [25]. To prepare functionalized GNp (FGNp), the acylation reaction was done by mixing of 20:1(v:v) thionyl chloride and DMF under ultrasonic condition for 2 hours at 70˚C in N_2 atmosphere. The obtained product was centrifuged at 4000rpm. To remove residual thionyl chloride, the FGNp was washed with dried THF and dried under vacuum at 40˚C for 24 hours.

2.3.Nanocomposites preparation

PCL and PLA pellets and nano powder were dried in a vacuum oven overnight before using. Specified amounts of the FGNp (075 and 1.5 wt%) were added to the dried DMF and stirred at room temperature. To obtain uniform suspension, the mixture was under ultrasonic treatment. At the same time, the PLA and PCL were dissolved in the dried DMF separately. Then the PLA solution was added to the suspension of FGNp and stirred for 4 hours. In the next step, PCL was added to the suspension. In order to get better dispersion, the DCP and TAIC were dissolved in dried DMF and then added to the mixture of PLA. After complete mixing, the solvent was evaporated at high temperature and was kept in a vacuum oven for 4 days to eliminate the solvent entirely. The obtained films were compression molded at 180˚C to accomplish the cross-linking reaction.

2.4.Characterizations

Fourier transform infrared spectroscopy (FTIR) (Bruker EQUINOX 55) was done in the 400-4000cm^{-1} range. Raman spectroscopy (LaRam Aramis) was performed at room temperature using a 532nm laser. Thermogravimetric analysis (TGA) was accomplished by using a TA instruments Q500. The morphology of GNps was observed using a scanning transmission electron microscopy (STEM) (FEI, Nova NanoSEM 450) on accelerating voltage of 15 kV.

Differential scanning calorimetry **(**DSC**)** (DSC 2010 from TA instruments) analysis was performed under nitrogen atmosphere. In the first heating cycle, the samples were heated to 250˚C at a rate of 5˚Cmin^{-1} and annealed at this temperature for 5 minutes to remove prior thermal history. Afterward, the samples were cooled to -30˚C using scan rate of 5˚Cmin^{-1} in the cooling cycle. In the second heating cycle, the samples were reheated to 250˚C at a rate of 5˚Cmin^{-1}. The status of nanoparticles in the samples was characterized using transmission electron microscopy (TEM) (FEI Tecnai transmission electron microscopy) at an accelerating voltage of 200kV. The evaluation of crystallinity percentage of phases in the heating-cooling steps was done by variable temperature X-ray diffraction (VT-XRD) (Philips X'Pert PRO Diffractometer) at different temperatures with scanning rate 10˚Cmin^{-1}. A triple-shape memory testing was applied on the rectangular specimens of approximately 20mm × 5mm × 1mm dimensions. All the thermomechanical programs for shape memory induction were carried out with a stress-controlled DMA (Q800, TA instruments) in tension mode. The thermal programs are schematically illustrated in Fig. 1. As can be seen, in the step 1, the sample (shape A) was first heated to a high-temperature T_{high} (165˚C) and kept for 10 minutes under a low tensile stress of 0.001N to allow stress relaxation before extending. Then, the stress-controlled uniaxial stretching was applied and was kept constant during subsequent quenching. In the step 2, the sample was cooled to a middle-temperature T_{mid} (70˚C) to fix the first temporary shape which obtained in the previous step. After removing the applied stress, a shape B is formed. In the step 3, similar to the step 1, after being kept for another 10 minutes at T_{mid} the sample was extended again. In the step 4, after cooling the sample to a low-temperature T_{low} (0˚C), a shape C was obtained upon releasing the external stress. In the step 5, a free strain recovery was performed

under continuous re-heating to T_{mid} at 5˚Cmin^{-1} to return to shape B. Finally in the step 6, when the sample was further heating continue to T_{high}, the original shape was recovered.

Regarding to the thermal-mechanical programming in Fig. 1, the shape fixity (R_f) and shape recovery (R_r) ratios were calculated according to equations 1-5 [26].

$$(\%)\ R_{f,\ A\to B} = \frac{\varepsilon^1_{f(N)} - \varepsilon^2_{p(N-1)}}{\varepsilon^1_{d(N)} - \varepsilon^2_{p(N-1)}} \times 100 \quad (1) \qquad (\%)\ R_{f,\ B\to C} = \frac{\varepsilon^2_{f(N)} - \varepsilon^1_{f(N)}}{\varepsilon^2_{d(N)} - \varepsilon^1_{f(N)}} \times 100 \quad (2)$$

$$(\%)\ R_{r,\ C\to B} = \frac{\varepsilon^2_{f(N)} - \varepsilon^1_{p(N)}}{\varepsilon^2_{f(N)} - \varepsilon^1_{f(N)}} \times 100 \quad (3) \qquad (\%)\ R_{r,\ B\to A} = \frac{\varepsilon^1_{f(N)} - \varepsilon^2_{p(N)}}{\varepsilon^1_{f(N)} - \varepsilon^2_{p(N-1)}} \times 100 \quad (4)$$

$$(\%) R_{r,\ C\to A} = \frac{\varepsilon^2_{f(N)} - \varepsilon^2_{p(N)}}{\varepsilon^2_{f(N)} - \varepsilon^2_{p(N-1)}} \times 100 \quad (5)$$

Here, $\varepsilon^2_{p(N-1)}$ is equal to the original strain ($\varepsilon_{p(0)}$) of shape A. $\varepsilon^1_{d(N)}$ and $\varepsilon^1_{f(N)}$ are the engineering strain after uniaxial stretching in step 1 and after unloading in step 2 respectively. $\varepsilon^2_{d(N)}$ is the engineering stain after uniaxial stretching in step 3 and $\varepsilon^2_{f(N)}$ is the engineering strain of shape C after unloading in step 4. $\varepsilon^1_{p(N)}$ is the engineering strain of recovered shape B in step 5 and $\varepsilon^2_{p(N)}$ denotes the engineering strain of original shape (shape A) in step 6.

3. Results and discussion

3.1. Characterization of functionalized GNps

Fig. 2(a) shows the FTIR spectra of nanoparticles. As can be seen, a small peak at 3431cm^{-1} was observed which corresponded to hydroxyl groups in pristine GNp. This peak was intensified after the functionalization reactions in OGNp and FGNp, which implies to formation of new hydroxyl groups. In addition, the peaks at 1713, 1389 and 1170cm^{-1} appeared in OGNp can be a reflection of the formation of carbonyl groups. These peaks are attributed to carboxylic acids (-COOH-), asymmetric –COO- stretch and symmetric –COO- stretch, respectively. After the acylation reaction and produces chlorine-containing functional group on the surface of FGNp, a

peak at 600cm^{-1} was appeared indicating that a successful reaction of acylation is done. Similar results have been reported by other researcher [28]. The Raman spectra for pristine GNp and functionalized samples are illustrated in Fig. 2(b). In these spectra, three distinguished bands can be seen: D band, G band, and 2D band become visible around 1335, 1580 and 2660cm^{-1}, respectively. The structural defects of GNps play a crucial role in the final properties of this filler and their nanocomposites. It is well known that the intensity ratio can be used as an indicator of structural defects quantity [28]. The lower I_D/I_G value means the fewer the defects, in the other words, by making progress of the functionalization reaction, the amount of defects increase. FGNp shows an I_D/I_G value of 0.58, which is higher than that of OGNp (0.49), indicating more defects and confirming the functionalization reaction. The TGA thermograms of samples are shown in Fig. 2(c). In all the thermograms, with increasing the temperatures, two main weight loss steps appeared. The first step of weight loss around 100˚C is related to the evaporation of physically absorbed water while the second step around 200˚C is depended to the pyrolysis of oxygen- containing groups [25]. In the range of 180-220˚C, the weight losses were 3, 11, and 8% for GNp, OGNp, and FGNp, respectively. The difference in the thermal behavior of the samples probably related to the existence of oxygen-containing group on the surface of OGNp and FGNp. In comparison to neat GNp, during the functionalization reactions some organic groups create on the surface of modified GNp and in this range (180-220˚C) these groups gradually decomposed. Indicative STEM images of GNp, OGNp, and FGNp dispersed in the solvent are shown in Fig. 3. The images indicated that GNp particles tend to aggregates while OGNp reveals more homogenous with low tendency to aggregation and FGNp illustrates more individual plates. By considering the results of FTIR, Raman, TGA and STEM tests, it can be concluded that the functionalization reactions are successfully accomplished.

3.2. Determination of chemical cross-linking linkage

The presence of cross-linking linkage can be demonstrated by gel content measurements. In this study, gel content was determined similar to cross-linked ethylene plastic according to ASTM D2765. All the samples showed approximately the same gel content (≈ 98%), meaning that the cross-linking had been successful in the samples. The samples containing 70 wt% PLA showed a better response to the applied cross-linking system. Cross-linking the PLA chains in the amorphous phase increased the cross-linking linkages at the ends of the chain and prevented them from decomposition at the melting point [29, 30].

3.3. Nanocomposite characterization

Typical TEM micrographs of samples containing 1.5 wt% OGNp and FGNp in PLA50/PCL50 matrix are demonstrated in Fig. 4. The effect of functionalization on the FGNps is clear. As it is seen transparent graphene nanoplatelets, which may be contain even monolayer graphene, can be clearly observed in comparison to OGNp. It is evident from the image that FGNps were homogenously dispersed in the matrix and the exfoliated state is acceded, furthermore the folded sheets of FGNps were observed to be well dispersed in the polymeric matrix. Since PLA and PCL are semi-crystalline polymers, their shape memory properties are strongly affected by crystallization. In order to consider the influence of GNp loading and modification reactions on the crystallinity of the nanocomposites, DSC was employed. Fig. 5 shows the typical DSC thermograms of the nanocomposites of PLA50/PCL50 in cooling and second heating steps and the obtained data are listed in Table 1. As can be seen, in the cooling step in PLA/PCL samples without nanoparticles, PLA (due to a low rate of crystallization kinetic) can not show any crystallization peak by a rate of $5^{\circ}Cmin^{-1}$. During second heating the blends showed two melting peaks at 50 and 159˚C, which are related to the PCL and PLA respectively. It indicates the

thorough immiscibility between the PLA and PCL phases in the blends. In addition the degree of crystallinity (X_c) for PLA was about 3%. In the nanocomposites, the addition of FGNps did not significantly change the melting points of the PLA and PCL. The two melting peaks are at 51˚C and 160˚C respectively, which are very close to that of the pure component. However, there is a notable increased in degree of crystallinity of PLA phase with increasing the loading of FGNp. Moreover, for PLA/PCL/FGNp nanocomposites in all composition ratios, $X_{c,\ PLA}$ was increased by 0.2-12% for different FGNps loading, while this increase was more significant for PLA70/PCL30/FGNp 1.5 nanocomposites with an increase of 4-22%. It can be conclude that, by incorporating the nanoparticles into blends, the crystallization peaks appeared which indicates that these nanoparticles act as nucleation agent and enhanced the crystallization process.

3.4. Shape memory behavior

The triple-shape memory properties were examined under a controlled-force mode in film tension according to the thermomechanical cycle aforesaid in the previous section. The melting points of crystalline phases were selected as transition temperatures (T_{trans}) and triple-shape memory was induced at $T_{m,\ PLA}$ and $T_{m,PCL}$. Fig. 6 shows the typical time dependence of strain, stress and temperature during the triple-shape memory cycle for PLA50/PCL50 blend and the samples containing 0.75 and 1.5 wt% FGNp. The fixity and recovery ratios (R_f and R_r) as the main indices of shape memory performance according to equations 1 to 5 were calculated and summarized in Table 2. The process is divided into stretching and recovery steps. As can be seen, in Fig 6a at the stretching step, when stress (1MPa) is loaded at 165˚C, the strain value is increased to 18.4% quickly. During the cooling to 65˚C under the load, the strain remains constant approximately. As the stress is unloaded, the strain decreases slightly to 16.4% and the first temporary shape is formed. Afterward, the stress (3MPa) is applied at 65˚C in which the

strain reaches to 31.4% quickly. During the cooling to 0˚C under the load, the strain does not change. After removing the stress, the strain decreases further to 30.1% and the second temporary shape is obtained. To recover the aforementioned shapes, the heating process under unload condition is applied in two steps. The strain returns to 19.5% and 7.9% at 65 and 165˚C respectively. Considering the fact that the strain is still recovering under keeping at the isothermal condition and the recovery ratio is increasing, the sample stay at 65˚C and 165˚C for 10 minutes. The same procedure was conducted to the samples containing 0.75 and 1.5 wt% FGNp which one can find in Fig. 6b and c. Regarding to Table 2, the shape fixity ratios (R_f) of PLA50/PCL50 were increased from 89.7 to 95.8% from A→B and 91.4 to 96.3% from B→C by addition of 1.5 wt% FGNp. All PLA/PCL nanocomposite samples showed fixity ratios higher than 80%. In addition, recovery ratios were in the range of 60-90%. Two factors control the shape memory properties which is consisting the movement of soft phase and the modulus of hard phase [31]. In this study, cross-linked PLA/PCL blends are T_m-based SMP in which PLA gives the hard phase for the shape fixity and PCL supplies the reversible phase for the shape recovery. Consequently, high fixity ratio illustrates that the temporary shape is reserved based on vitrification of soft phases during cooling. The shape fixity of SMP is dictated by two factors [32]. The first is the amount of unlocked oriented chains for which the orientation of these stretched chains is maintained by crystallization and cross-link linkage in the cooling stage. The second is the modulus of the material which be less, low values of shape fixity occurred. So, the shape fixity was increased which may be attributed to the enhancing of the crystallization and modulus of the samples. Our data indicate that by incorporation of FGNp (Table 2), the shape fixity was increased. This observation is in agreement with presented DSC data in previous section. During the recovery step, when the stress was removed, the reversible phase gradually

restored and relaxed to the original structure. So the value of shape recovery of blends follow similar trends as shape fixity and shows sensitively to the nanoparticles content.

It can be concluded that in the shape memory programming, at high stretching temperature (165˚C) both polymeric chains oriented, whereas at low stretching temperature (65˚C) only the chains of PCL phase oriented. During the cooling step, these two phases maintained their oriented domains due to being in the glassy state. When the stress was unloaded, first the PCL chains recovered and then the PLA chains returned at 65˚C and 165˚C respectively. It is important to note that the polymeric phases could not be recovered completely because of some irreversible deformations and chain slippages. Another point which should be considered that the shorter time recovery was achieved for the nanocomposite samples due to presence of FGNps as a thermal conductive filler.

3.5. Variable-temperature X-ray diffraction study

Since the crystallization of the phases plays an important role in the shape memory performance, the VT-XRD was used to get better understanding of the effect of graphene nanoparticles on the crystallization behavior in the heating and cooling steps of programming triple-SMPs. At the room temperature, the PLA shows the strongest reflection indices (200) at 2θ= 16.4˚ and (203) at 2θ= 18.6˚ and PCL (110) at 2θ= 21.6˚ and (200) at 2θ= 23.8˚ [33]. As mentioned in the experimental section, VT-XRD analysis was accomplished at 25˚C, 70˚C, 80˚C, 90˚C and cooled at 25˚C. At theses temperatures PLA crystals do not change appreciably while the PCL phase experiences some different levels of crystallinity. In other words, in this test the crystallization percentage of PCL phase was evaluated *in situ* during heating the samples to 90˚C and subsequently cooling to room temperature (25˚C) at constant rate. The typical VT-XRD patterns of PLA50/PCL50 and PLA50/PCL50/FGNp 1.5 are depicted in Fig. 7. As can be seen in Fig. 7a,

at room temperature the crystallinity peaks of both PLA and PCL are clearly detected. The intensity of PCL peaks decreased with increasing temperature and disappeared completely at 90ºC, where the PLA peaks did not change during the thermal cycling. By cooling the blend samples to 25˚C and repeating the XRD analysis, the PCL peaks were appeared with lower intensity which means re-crystallization was not completely occurred. It is probably, because of lack of heat transfer in the thermally actuation stage which affect the relaxation time and the crystallization kinetic. It seems controlling the shape fixity and shape recovery can be affected by these phenomena. Therefore, low conductivity of polymer reduces the shape memory performance [34]. In this study, quantitative phase analysis by the XRD, based on the fact that the volume fraction of any crystalline phase in a blend, was calculated from the measured integrated intensities of diffracted peaks [35]. The results of quantitative phase analysis of the PCL that extracted from diffractograms are disclosed in Table 3. Regarding to Table 3, by addition of graphene nanoplatelets into the blends, the PCL crystallization percentage in the total sum of all crystalline phases decreased. It may be due to the impressive effect of FGNps on the PLA crystallization in compare to PCL which causes a decrease in the crystallization amount of PCL phase. It seems the main reason for more effect of FGNps on the PLA phase crystallization is the selective localization of these nanoparticles in the PLA phase due to better matching by its functionalization. As mentioned before, an improvement of re-crystallization can be attributed to the raising the heat transfer owing to presence of FGNps.

4. Conclusion

This study is motivated by current researches in the field of triple-SMPs nanocomposites. In this work, thermally actuated triple-SMPs of chemically cross-linked PLA/PCL/FGNp nanocomposites were prepared by facile solution mixing method. The morphology and also the

thermal and shape memory properties were investigated. TEM analysis revealed that the FGNp had good interactions with matrix and were completely exfoliated so increase the crystallinity which resulted in an improvement in shape memory performance. The samples showed two-well separated transition temperatures corresponding to melting points of PLA and PCL phases. Two temporary shapes were fixed at 65 and 0˚C, which recovery at 65 and 165˚C. The triple-SMPs by immiscible PLA/PCL blends with 50 wt% PLA showed pronounced triple-SMPs in DMA analysis. This novel strategy of cross-linked immiscible blends could be applied to design and prepare new triple-SMPs based on melting temperature of polymers. Incorporating of the FGNp into the blends increases the shape fixity because of enhancing of the crystallization and modulus of the samples. Furthermore, in the presence of thermal conductive FGNp, high recovery ratio was achieved. The greatest shape memory behavior was obtained for the samples of PLA50/PCL50 containing 1.5 wt% FGNps.

References

[1] S. Abdallah-Elhirtsi, J. Fitoussi, B.J. Rashmi, K. Prashantha, S. Farzaneh, M.F. Lacrampe, P. Krawczak, A. charkhtchi, Study of partial shape memory effect of polymers by multicycle tests, Polym. Compos. 36 (2015) 1145-1151.

[2] H. Kalita, N. Karak, Bio-based hyperbranched polyurethane/Fe_3O_4 nanocomposites as shape memory materials, Polym. Adv. Technol. 24 (2013) 819-823.

[3] B. Yan, S. Gu, Y. Zhang, Polylactide-based thermoplastic shape memory polymer nanocomposites, Eur. Polym. J. 49 (2013) 366-378.

[4] M. Behl, U. Ridder, Y. Feng, S. Kelchd, A. Lendlein, Shape-memory capability of binary multiblock copolymer blends with hard and switching domains provided by different components, Soft Matter 5 (2009) 676-684.

[5] J. Hu, Y. Zhu, H. Huang, J. Lu, Recent advances in shape–memory polymers: structure, mechanism, functionality, modeling and applications, Prog. Polym. Sci. 37 (2012) 1720-1763.

[6] Q. Zhang, W. Hua, J. Feng, a facile strategy to fabricate multishape memory polymers with controllable mechanical properties, Macromol. Rapid Commun. 37 (2016) 1262-1267.

[7] J. Zotzmann, M. Behl, D. Hofmann, A. Lendlein, Reversible triple-shape effect of polymer networks containing polypentadecalactone- and poly(ε-caprolactone)-segments, Adv. Mater. 22 (2010) 3424–3429.

[8] F. Pilate, R. Mincheva,; J.D. Winter, P. Gerbaux, L. Wu, R. Todd, J.M. Raquez, P. Dubois, Design of multistimuli-responsive shape-memory polymer materials by reactive extrusion, Chem. Mater. 26 (2014) 5860-5867.

[9] T. Zhang, Z. Wen, Y. Hui, K. Yang, Q. Zhou, Y. Wang, Facile fabrication of a well-defined poly(p-dioxanone) dynamic network from metallosupramolecular interactions to obtain an excellent shape-memory effect, Polym. Chem. 6 (2015) 4177-4184.

[10] U. Nöchel, U.N. Kumar, K. Wang, K. Kratz, M. Behl, A. Lendlein, Triple-shape effect with adjustable switching temperatures in crosslinked poly[ethylene- co - (vinyl acetate)], Macromol. Chem. Phys. 215 (2014) 2446-2456.

[11] J. Zhao, M. Chen, X. Wang, X. Zhao, Z. Wang, Z.M. Dang, L. Ma, G.H. Hu, F. Chen, Triple shape memory effects of cross-linked polyethylene/polypropylene blends with cocontinuous architecture, ACS Appl. Mater. Interfaces5 (2013) 5550-5556.

[12] S.Y. Gu, L.L. Liua, X.F. Gaoa, Triple-shape memory properties of polyurethane/polylactide-polytetramethylene ether blends, Polym. Int. 64 (2015) 1155-1162.

[13] S. Chatani, C. Wang, M. Podgorski, C.N. Bowman, Triple shape memory materials incorporating two distinct polymer networks formed by selective thiol−michael addition reactions, Macromolecules 47 (2014) 4949-4954.

[14] X. Luo, P.T. Mather, Triple-shape polymeric composites (TSPCs), Adv. Funct. Mater. 20 (2010) 2649-2656.

[15] H. Kalita, N. Karak, Bio-based hyperbranched polyurethane/multi-walled carbon nanotube nanocomposites as shape memory materials, Polym. Compos. 35 (2014) 636-643.

[16] B. Xu, W.M. Huang, Y.T. Pei, Z.G. Chen, A. Kraft, R. Reuben, J.Th.M. De Hosson, Y.Q. Fu, Mechanical properties of attapulgite clay reinforced polyurethane shape-memory nanocomposites, Eur. Polym. J. 45 (2009) 1904-1911.

[17] F. Memarian, A. Fereidoon, M.G. Ahangari, H.A. Khonakdar, Shape memory and mechanical properties of TPU/ABS blends: The role of pristine versus organo-modified carbon nanotubes, Polym. Compos. 2017, DOI:10.1002/pc.24387.

[18] S. Lashgari, M. Karrabi, I. Ghasemi, H. Azizi, M. Messori, K. Paderni, Shape memory nanocomposite of poly(l-lactic acid)/graphene nanoplatelets triggered by infrared light and thermal heating, Express. Polym. Lett. 10 (2016) 349-359.

[19] S. Lashgari, M. Karrabi, I. Ghasemi, H. Azizi, M. Messori, Graphene nanoplatelets dispersion in poly(l-lactic acid): Preparation method and its influence on electrical, crystallinity and thermomechanical properties, Iran. Polym. J. 25 (2016) 193-202.

[20] M. Sabzi, M. Babaahmadi, N. Samadi, G.R. Mahdavinia, M. Keramati, N. Nikfarjam, Graphene network enabled high speed electrical actuation of shape memory nanocomposite based on poly(vinyl acetate), Polym. Int. 66 (2017) 665-671.

[21] Z. Zhang, J. Dou, J. He, C. Xiao, L. Shen, J. Yang, Y. Wang, Z. Zhou, Electrically/infrared actuated shape memory composites based on a bio-based polyester blend and graphene nanoplatelets and their excellent self-driven ability, J. Mater. Chem. C 5 (2017) 4145-4158.

[22] M. Babaahmadi, M. Sabzi, G.R. Mahdavinia, M. Keramati, Preparation of amorphous nanocomposites with quick heat triggered shape memory behavior. Polym. 112 (2017) 26-34.

[23] M. Keramati, I. Ghasemi, M. Karrabi, H. Azizi, M. Sabzi, Dispersion of graphene nanoplatelets in polylactic acid with the aid of a zwitterionic surfactant: evaluation of the shape memory behavior, Polym. Plast. Technol. Eng. 55 (2016) 1039-1047.

[24] M. Keramati, I. Ghasemi, M. Karrabi, H. Azizi, M. Sabzi, Incorporation of surface modified graphene nanoplatelets for development of shape memory PLA nanocomposite, Fiber. Polym. 17 (2016) 062-1068.

[25] P. Manafi, I. Ghasemi, M. Karrabi, H. Azizi, M.R. Manafi, P. Ehsaninamin, Thermal stability and thermal degradation kinetics (model-free kinetics) of nanocomposites based on poly (lactic acid)/graphene: the influence of functionalization. Polym. Bull. 72 (2015) 1095-1112.

[26] Q. Zhao, H.J. Qi, T. Xie, Recent progress in shape memory polymer: new behavior, enabling materials, and mechanistic understanding, Prog. Polym. Sci. 49-50 (2015) 79-120.

[27] N.A. Kumar, H.J. Choi, Y.R. Shin, D.W. Chang, L. Dai, J.B. Baek, Polyaniline-grafted reduced graphene oxide for efficient electrochemical supercapacitors, ACS Nano 6 (2016) 1715-1723.

[28] Y. Gao, O.T. Picot, E. Bilotti, T. Peijs, Influence of filler size on the properties of poly(lactic acid) (PLA)/graphene nanoplatelet (GNP) nanocomposites, Eur. Polym. J. 86 (2017) 117-131.

[29] H. Bai, H. Liu, D. Bai, Q. Zhang, K. Wang, H. Deng, F. Chena, Q. Fu, Enhancing the melt stability of polylactide stereocomplexes using a solid-state cross-linking strategy during a melt-blending process, Polym. Chem. 5 (2014) 5985-5993.

[30] S.I. Yang, Z.H. Wu, W. Yang, M.B. Yang, Thermal and mechanical properties of chemical crosslinked polylactide (PLA), Polym. Test. 27 (2008) 957-963.

[31] A. Abbasi, G. M.M.Sadeghi, I. Ghasemi, M. Sahrousvand, Shape memory performance of green *In situ* polymerized nanocomposites based on polyurethane/graphene nanoplatelets: synthesis, properties, and cell behavior, Polym. Compos. 2017, DOI: 10.1002/pc.24456.

[32] I.S. Gunes, F. Cao, S.C. Jana, Evaluation of nanoparticulate fillers for development of shape memory polyurethane nanocomposites, Polym. 49 (2008) 2223-2234.

[33] J.T. Yeh1, C.J. Wu, C.H. Tsou, W.L. Chai, J.D. Chow, C.Y. Huang, K.N. Chen, C.S. Wu, Study on the crystallization, miscibility, morphology, properties of poly(lactic acid)/poly(ε-caprolactone) blends, Polym. Plast. Technol. Eng. 48 (2009) 571-578.

[34] Z. Tang, D. Sun, D. Yang, B. Guo, L. Zhang, D. Jia, Vapor grown carbon nanofiber reinforced bio-based polyester for electroactive shape memory performance, Compos. Sci. Technol. 75 (2013) 15-21.

[35] Z. Pala, E. Shaw, J.W. Murray; N. Senin, T. Hussain, Suspension high velocity oxy-fuel spraying of Tio_2: A quantitative approach to phase composition, J. Eur. Ceram. Soc. 37 (2017) 801-810.

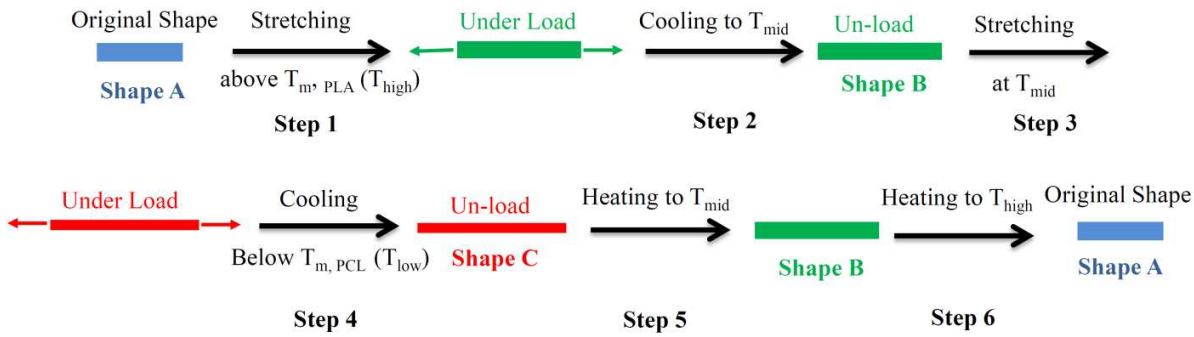

Fig. 1. Schematic description of a triple-shape memory programming

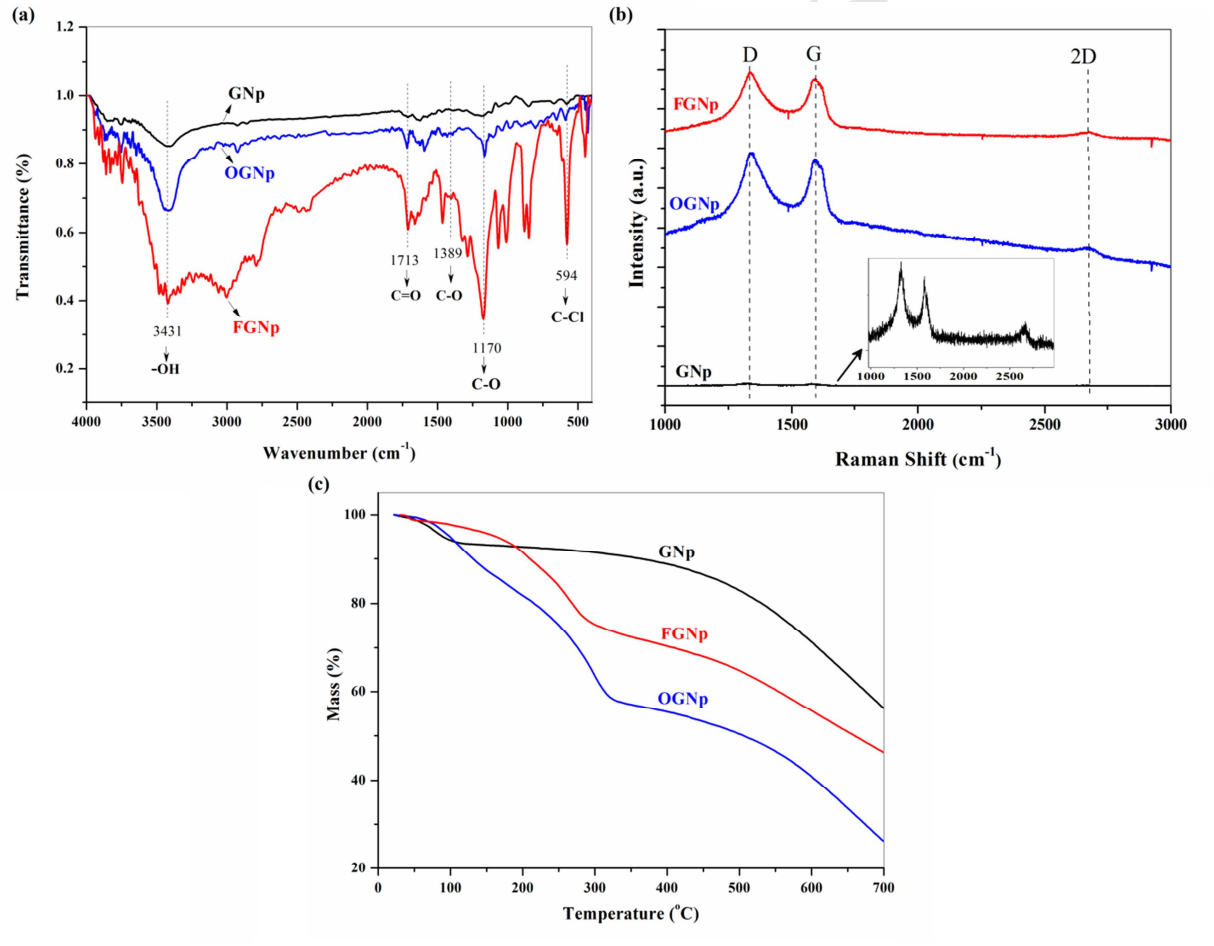

Fig. 2. (a) FTIR spectra, (b) Raman spectra and (c) TGA thermograms of GNp, OGNp, and FGNp nanoparticles.

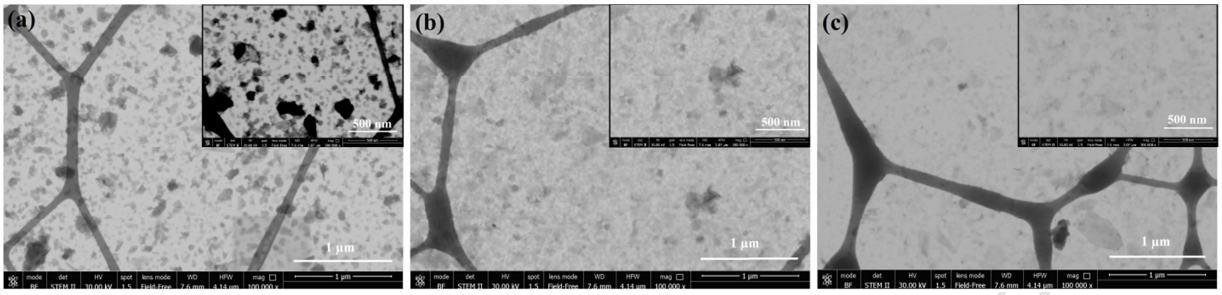

Fig. 3. STEM images of graphene nanoparticles dispersed in the DMF solvent: (a) GNp, (b) OGNp, and (c) FGNp

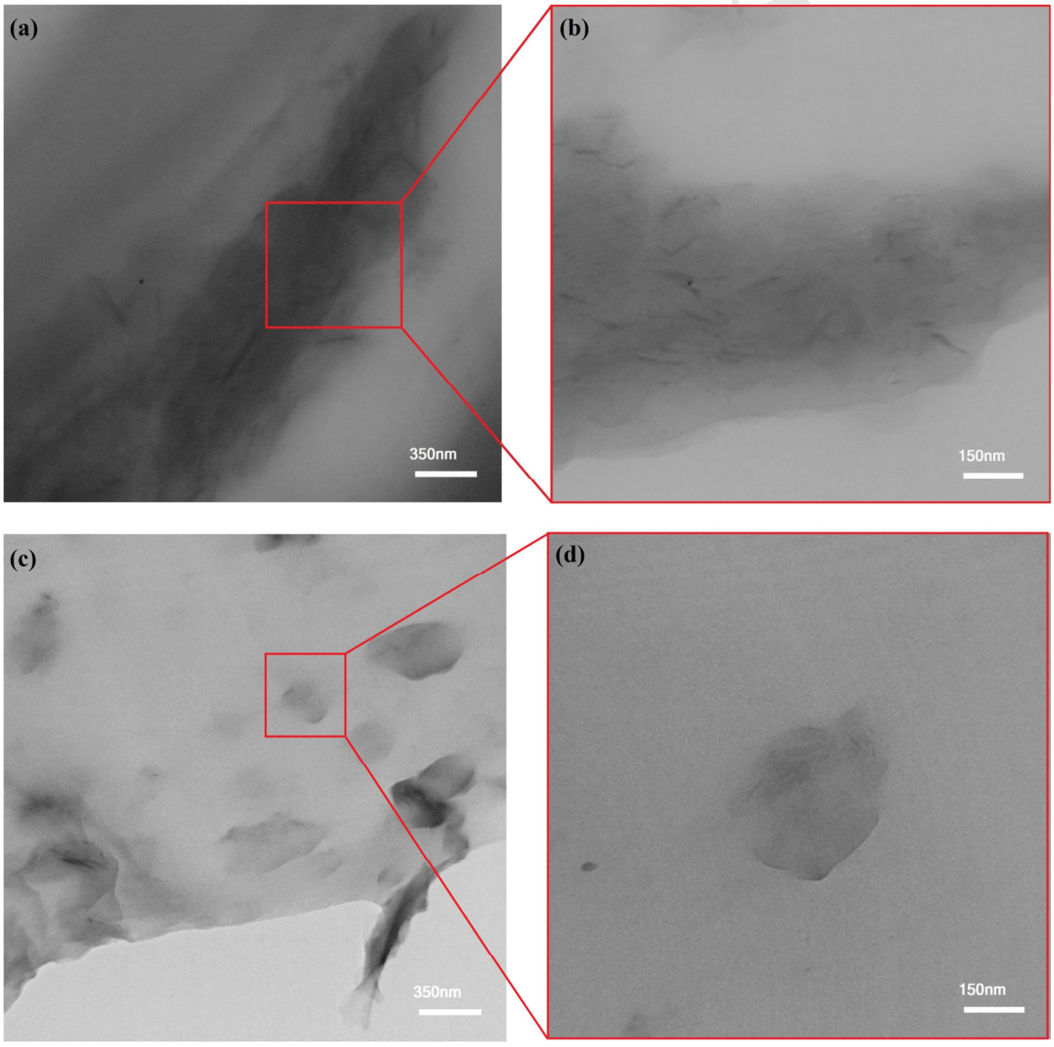

Fig. 4 Typical TEM images of (a,b) OGNp and (c,d) FGNp (1.5 wt%) in PLA50/PCL50 matrix

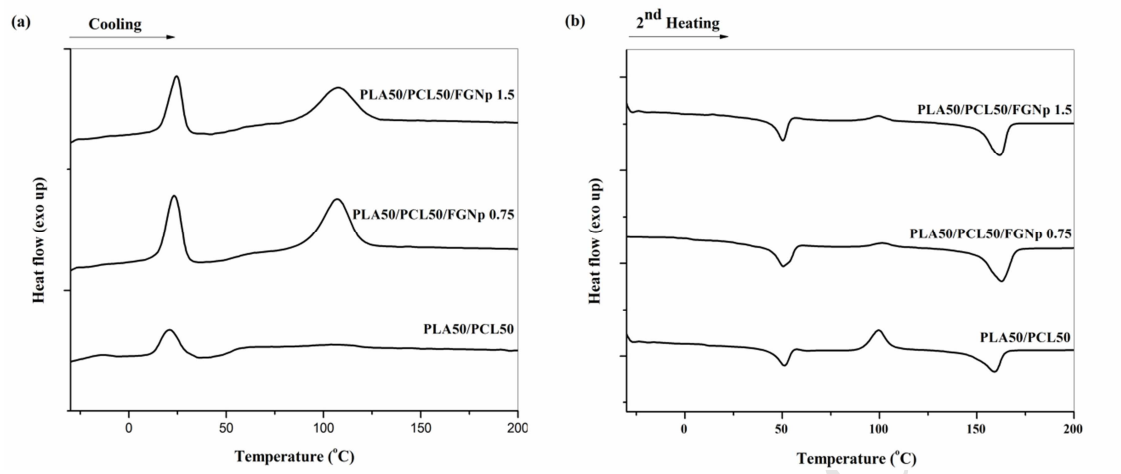

Fig. 5. DSC thermograms of nanocomposites of PLA50/PCL50 at 5˚Cmin^{-1} (a) cooling, (b) second heating

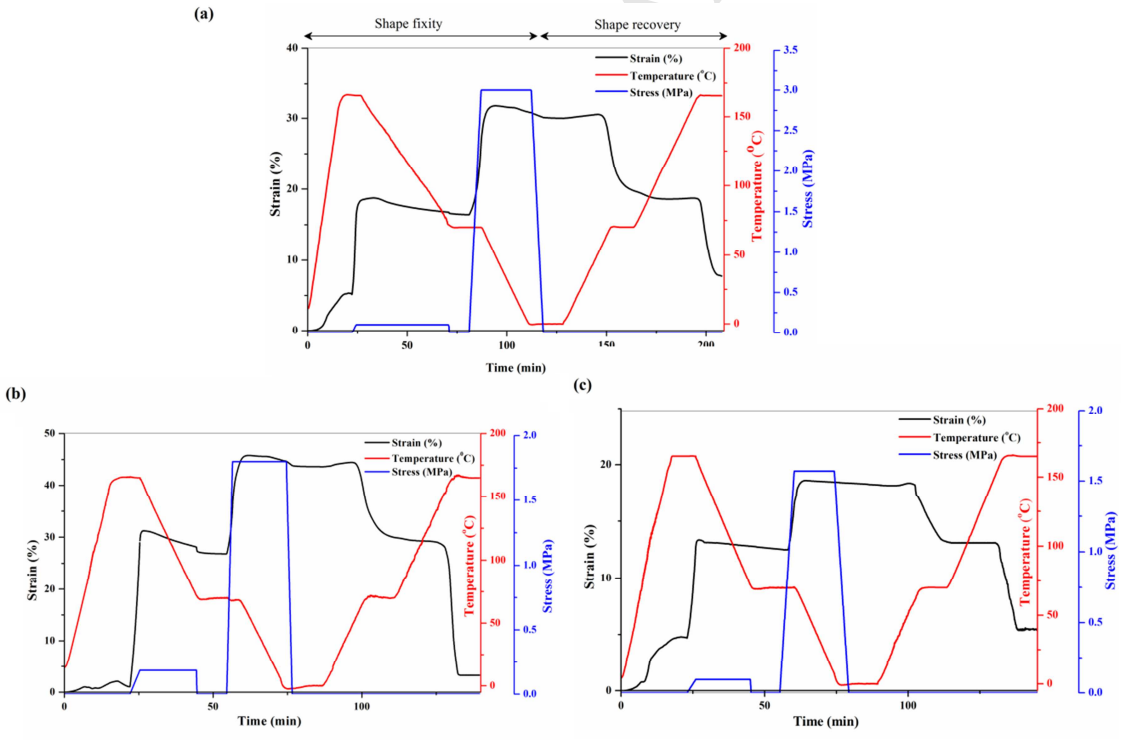

Fig. 6. Triple-shape memory cycles of PLA/PCL blend: (a) PLA50/PCL50, (b) PLA50/PCL50/FGNp 0.75, (c) PLA50/PCL50/FGNp 1.5

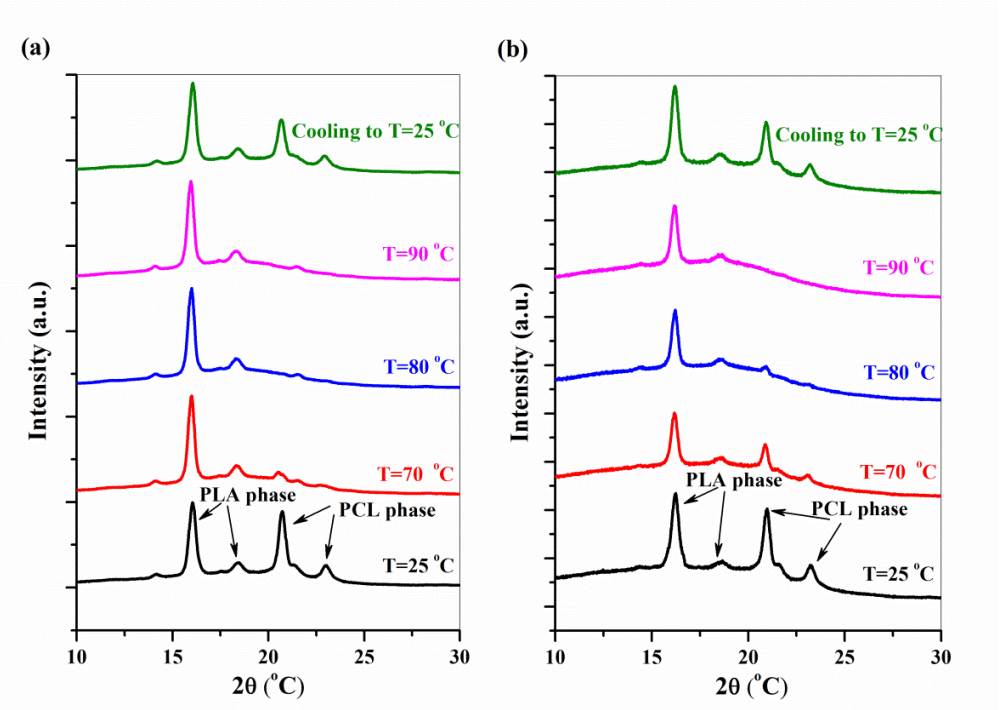

Fig. 7 VT-XRD patterns of PLA50/PCL50 blend at heating-cooling cycle: (a) PLA50/PCL50, (b) PLA50/PCL50/FGNp 1.5

Table 1 Summarized the DSC analysis of the PLA/PCL/GNp nanocomposites

Sample Name	Cooling				2nd Heating				
	$T_{c,PCL}$ (˚C)	$T_{c,PLA}$ (˚C)	$\Delta H_{c,PLA}$ (J/g)	$X_{c,PLA}$ (%)	$T_{cc,PL}$ $_{A}$ (˚C)	$T_{m,PLA}$ (˚C)	$T_{m,PCL}$ (˚C)	$\Delta H_{cc,,PLA}$ (J/g)	$\Delta Hm_{,PLA}$ (J/g)
PLA30/PCL70	23.2	-	-	2.1	94.9	156.9	51.9	3.8	4.7
PLA30/PCL70/FGNP 0.75	25.3	116.3	1.2	12.7	97.6	162.2	53.5	3.2	6.4
PLA30/PCL70/FGNP 1. 5	25.1	117.1	2.7	18.1	96.4	162.4	52.0	3.1	6.4
PLA50/PCL50	22.2	-	-	1.4	94.1	157.4	50.5	8.5	9.2
PLA50/PCL50/FGNP 0.75	24.4	107.9	2.7	15.1	99.1	160.2	50.9	6.1	9.7
PLA50/PCL50/FGNP 1. 5	21.8	112.5	7.3	20.9	99.3	160.6	50.8	3.3	11.4
PLA70/PCL30	20.8	-	-	3.0	99.5	158.9	50.9	9.9	11.8
PLA70/PCL30/FGNp 0.75	23.1	106.9	11.2	21.3	102.5	162.5	50.3	1.5	14.8
PLA70/PCL30/FGNp 1. 5	24.6	107.4	12.9	24.4	99.9	161.6	50.4	1.9	17.2

Table 2 Triple-shape memory performance of PLA/PCL blends recorded from cyclic thermal-mechanical tests carried on DMA

Sample Name	$R_{f, A\rightarrow B}$ (%)	$R_{f, B\rightarrow C}$ (%)	$R_{r, C\rightarrow B}$ (%)	$R_{r, B\rightarrow A}$ (%)	$R_{r,tot, C\rightarrow A}$ (%)
PLA30/PCL70	74.7	71.6	91.2	73.4	82.5
PLA30/PCL70/FGNp 0.75	77.4	83.4	93.2	75.8	85.2
PLA30/PCL70/FGNp 1.5	80.5	84.6	95.2	77.6	87.4
PLA50/PCL50	85.6	88.9	80.5	79.8	89.9
PLA50/PCL50/FGNp 0.75	89.7	91.4	88.7	91.2	94.3
PLA50/PCL50/ FGNp 1.5	95.8	96.3	93.4	94.6	96.7
PLA70/PCL30	92.9	71.4	27.5	81.8	79.7
PLA70/PCL30/FGNp 0.75	98.1	81.9	57. 4	83.5	84.3
PLA70/PCL30/FGNp 1.5	98.8	82.2	65.7	93.7	94.1

Table 3 Quantitative phase analysis of crystalline PCL phase from X-ray diffractograms

Samples Name	Percentage of crystalline PCL phase in total sum of all crystalline phases	
	at 25 ˚C	at 25 ˚C after cooling
PLA30/PCL70	90.1	79.7
PLA30/PCL70/FGNp 1.5	87.9	84.4
PLA50/PCL50	51.0	22.3
PLA50/PCL50/FGNp 1.5	45.4	36.5
PLA70/PCL30	35.2	22.0
PLA70/PCL30/FGNp 1.5	27.3	23.6